



Published in final edited form as:

*Acta Biomater.* 2017 July 15; 57: 70–84. doi:10.1016/j.actbio.2017.05.028.

## Photothermal and photodynamic activity of polymeric nanoparticles based on $\alpha$ -tocopheryl succinate-RAFT block copolymers conjugated to IR-780

Raquel Palao-Suay<sup>a,b,†</sup>, Francisco M. Martín-Saavedra<sup>b,c,‡</sup>, María Rosa Aguilar<sup>a,b,\*</sup>, Clara Escudero Duch<sup>c</sup>, Sergio Martín-Saldaña<sup>a,d</sup>, Francisco J. Parra-Ruiz<sup>a,b</sup>, Nathan A. Rohner<sup>e</sup>, Susan N. Thomas<sup>e</sup>, Nuria Vilaboa<sup>c,b</sup>, and Julio San Román<sup>a,b</sup>

<sup>a</sup>Group of Biomaterials, Department of Polymeric Nanomaterials and Biomaterials, Institute of Polymer Science and Technology, CSIC, Madrid, Spain

<sup>b</sup>Networking Biomedical Research Centre in Bioengineering, Biomaterials and Nanomedicine, CIBER-BBN, Spain

<sup>c</sup>La Paz University Hospital-IdiPAZ, Paseo de la Castellana 261, 28046 Madrid, Spain

<sup>d</sup>Department of Otorhinolaryngology, Puerta de Hierro Majadahonda University Hospital, C/ Manuel de Falla, 1, 28222 Majadahonda

<sup>e</sup>George W. Woodruff School of Mechanical Engineering and Parker H. Petit Institute of Bioengineering and Bioscience, Georgia Institute of Technology, Atlanta, Georgia, USA

### Abstract

The aim of this work was the generation of a multifunctional nanopolymeric system that incorporates IR-780 dye, a near-infrared (NIR) imaging probe that exhibits photothermal and photodynamic properties; and a derivate of  $\alpha$ -tocopheryl succinate ( $\alpha$ -TOS), a mitochondria-targeted anticancer compound. IR-780 was conjugated to the hydrophilic segment of copolymer PEG-*b*-polyMTOS, based on poly(ethylene glycol) (PEG) and a methacrylic derivative of  $\alpha$ -tocopheryl succinate (MTOS), to generate IR-NP, self-assembled nanoparticles (NPs) in aqueous media which exhibit a hydrophilic shell and a hydrophobic core. During assembly, the hydrophobic core of IR-NP could encapsulate additional IR-780 to generate derived subspecies carrying different amount of probe (IR-NP-eIR). Evaluation of photo-inducible properties of IR-NP and IR-NP-eIR were thoroughly assessed *in vitro*. Developed nanotheranostic particles showed distinct fluorescence and photothermal behavior after excitation by a laser light emitting at 808 nm. Treatment of MDA-MB-453 cells with IR-NP or IR-NP-eIR resulted in an efficient internalization of the IR-780 dye, while subsequent NIR-laser irradiation led to a severe decrease in cell viability. Photocytotoxicity conducted by IR-NP, which could not be attributed to the

\*Corresponding author: mraguilar@ictp.csic.es; Group of Biomaterials, Institute of Polymer Science and Technology (ICTP-CSIC). C/ Juan de la Cierva, 3. 28006 Madrid. Tel: +34 915622900; Fax: +34 915644853.

†These authors contributed equally.

**Publisher's Disclaimer:** This is a PDF file of an unedited manuscript that has been accepted for publication. As a service to our customers we are providing this early version of the manuscript. The manuscript will undergo copyediting, typesetting, and review of the resulting proof before it is published in its final citable form. Please note that during the production process errors may be discovered which could affect the content, and all legal disclaimers that apply to the journal pertain.

generation of lethal hyperthermia, responded to an increase in the levels of intracellular reactive oxygen species (ROS). Therefore, the fluorescence imaging and inducible phototoxicity capabilities of NPs derived from IR-780-PEG-*b*-polyMTOS copolymer confer high value to these nanotheranostics tools in clinical cancer research.

## Keywords

IR-780; nanoparticles;  $\alpha$ -tocopheryl succinate; phototherapeutic

---

## 1. Introduction

The future of oncology relies on the development of multifunctional theranostic nanosystems which combine diagnostics tests, targeted therapies, and real-time monitoring in a single platform [1-3]. Due to their unique physical and chemical properties, nanoparticles (NPs) have been exhaustively explored as platforms to deliver imaging and therapeutic agents to target sites. A wide number of nanosized delivery vehicles have been tested for theranostic applications, including quantum dots, superparamagnetic iron oxides NPs, gold NPs, liposomes, or niosomes [4, 5]. Polymer-based NPs are expected to play a significant role in the dawning era of nanotheranostics for personalized medicine [4], as they have shown improved efficacy and selectivity of entrapped or conjugated agents *via* enhanced permeability and retention (EPR) effect or through a prolonged circulation half-life and sustained drug release [1, 6].

NIR fluorescence is frequently used for *in vivo* imaging due to the extremely low absorption and autofluorescence of biological tissues in the wavelength range from 700 to 1000 nm. These features of NIR energy significantly improve the image sensitivity, by minimizing background interference, as well as increasing tissue depth penetration. NIR dyes absorb NIR wavelengths to reach an excited singlet state being part of the energy dissipated in the form of fluorescence. Some energy of the excited singlet state can transit through vibronic relaxation or other non-radiative transitions pathways and transform into heat. If the rate of heat production exceeds that of heat dissipation within a tissue, the temperature would increase gradually to levels that cause cellular cytotoxicity [7]. Alternatively, the excited singlet state can move to a lower-energy excited triplet state via intersystem crossing. Under this condition, the triplet state can undergo two different reactions: it can react with a substrate through electron or hydrogen atom transfer reactions, producing free radicals and other reactive oxygen species (ROS) (type I reaction); or it can transfer its energy directly to ground-state triplet oxygen to form excited state singlet oxygen (type II reaction)[8, 9]. These products induce oxidation reactions with nearby biomacromolecules, leading to cell death. Therefore, NIR dyes can effectively be used as promising agents for photothermal (PTT) and photodynamic (PDT) therapies[10-12].

Most typical NIR-nanoabsorbers are inorganic compounds with a non-degradable nature, nonspecific biodistribution and poorly characterized bioretention, which lead to toxicity effects that hinder clinical translation[13, 14]. Organic NIR dyes such cyanine compounds are efficient NIR-absorbers that have high molar absorptivity, good photostability and ability

to emit strong fluorescence at the NIR range, acting simultaneously as fluorescent imaging and phototherapeutic agents. Having small molecular weights, NIR dyes can be excreted shortly after injection, lowering long-term toxicity concerns[13, 14].

IR-780 iodide is a lipophilic cation heptamethine dye with specific absorption peak at 780 nm. As result of the presence of a rigid cyclohexenyl ring in the heptamethine chain with a central chlorine atom, the photostability and quantum yield are increased in comparison to inorganic NIR nanoabsorbers based in noble metals (*e.g.* Au, Ag, Pt), metal oxides or carbon[15]. The most important drawbacks for the clinical use of IR-780 iodide are its poor solubility in physiological medium[16] and the low tolerance observed in *in vivo* models[17]. To overcome these limitations, IR-780 dye has been encapsulated into polymeric multifunctional micelles labeled with rhenium-188[18], silica NPs[19] or liposomes[20]. However, these vehicles are difficult to synthesize, non-biodegradable and exhibit inefficient photothermal behavior. Recently, IR-780 iodide has been encapsulated in the inner core of the heparin-folic acid conjugate through ultrasonic sound method[21] or in human serum albumin to form NPs by protein self-assembly[17]. These NPs increase the aqueous solubility of the dye by 1000-fold and reduce ten times its toxicity[17].

Synthetic polymer-based nanovehicles have been only scarcely explored to administer IR-780 iodide. In this sense, the IR-780 iodide structure has been modified using the central chlorine atom in order to conjugate a hydrophilic PEG<sub>2000</sub>, forming micelles that improved its water solubility[22]. The appropriate size of these micelles (~100 nm) favored its preferential tumor accumulation[23] that could be attributed to lower opsonization of the nanomaterial by the reticuloendothelial system (RES)[24] and lower renal filtration[25].

One of the most attractive possibilities of nanoassembly design based on polymeric and synthetic macromolecules, is the use of amphiphilic block copolymers that are typically obtained by controlled polymerization techniques[26]. Using reversible addition-fragmentation chain transfer polymerization (RAFT), we have recently synthesized block copolymers based on PEG<sub>8000</sub> and MTOS, a methacrylic derivative of  $\alpha$ -tocopheryl succinate ( $\alpha$ -TOS), forming bioactive self-assembled NPs[27]. Both the PEG-block and an appropriate MW of the block copolymer favored the cytotoxic activity of  $\alpha$ -TOS, a mitocan that selectively induces apoptosis of malignant cells by targeting mitochondria while exerting minimal toxicity towards normal cells and tissues[28]. Relatively slow uptake of  $\alpha$ -TOS by malignant cells, which relies on passive diffusion, is a limiting point for its efficient delivery[29, 30]. This drawback can be overcome using NPs derived from MTOS, that can entrap additional  $\alpha$ -TOS in their inner core to significantly increase the amount of drug that reaches the cell interior and thereby improving its cytotoxic potential[31]. Incorporation of IR-780 iodide on the surface of the polymeric NPs derived from MTOS may increase the selectivity of these nanosystems. The lipophilic cationic nature of IR-780 dye facilitates the penetration through mitochondrial membranes which have zeta potentials ranging between -120 and -160 mV[32, 33]. Cancer cells typically show a more hyperpolarized mitochondrial membrane potential than nonmalignant cells[34, 35]. IR-780 iodide preferentially accumulates into mitochondria of tumor cells [36]. Moreover, IR-780 shows high affinity for organic anion transporter peptides (OATPs), frequently overexpressed in tumor cells[36, 37].

The aim of this work was the preparation of NPs based in block copolymers of PEG<sub>8000</sub> and MTOS that incorporate IR-780 in order to enhance their photothermal and/or photodynamic properties and enable real-time monitoring of target tissue by NIR fluorescence. IR-780 was successfully conjugated to amphiphilic block copolymers COOH-PEG-*b*-polyMTOS. Formation of spherical NPs entrapping free IR-780 iodide by self-organized precipitation (SORP) was investigated, including a complete characterization of their physicochemical properties. The photothermal properties of nanoassemblies incorporating IR-780 were examined in detail. Finally, cellular uptake, anticancer and phototherapeutic activities of these NPs were evaluated *in vitro* using breast carcinoma cells (Fig. 1).

## 2. Materials and methods

### 2.1. Materials

MTOS and CTA-PEG<sub>8</sub> were obtained as previously described[27, 38]. 4-dimethylaminopyridine (DMAP, Sigma-Aldrich), triethylamine (Et<sub>3</sub>N, Scharlau) and succinic anhydride (SA, Sigma-Aldrich) were used without further purification in the modification of PEG macro-CTA agent. 1,4-dioxane anhydrous (Sigma-Aldrich) was used without further purification and 2,2'-Azobisisobutyronitrile (AIBN, Merck) was recrystallized from methanol (m.p. 104 °C) for the RAFT polymerization. 2-[2-[2-Chloro-3-[(1,3-dihydro-3,3-dimethyl-1-propyl-2H-indol-2-ylidene)ethylidene]-1-cyclohexen-1-yl]ethenyl]-3,3-dimethyl-1-propylindolium iodide (IR-780 iodide, Sigma-Aldrich), 4-(4,6-Dimethoxy-1,3,5-triazin-2-yl)-4-methylmorpholinium chloride (DMTMM, Sigma-Aldrich), tetrahydrofuran anhydrous (THF, Sigma-Aldrich), dimethylformamide anhydrous (DMF, Sigma-Aldrich) and ethanol (EtOH, Merck) were used without further purification in the preparation of IR-780 based polymer conjugate. Deuterated chloroform (CDCl<sub>3</sub>, Sigma-Aldrich) and chromatographic grade tetrahydrofuran (THF, Sigma-Aldrich) were used without further purification to characterize the polymeric conjugate. Additionally, sodium chloride (NaCl, Panreac) was used without further purification for the preparation of self-assembled NPs.

### 2.2. Preparation of IR-780-based NPs

**Synthesis of COOH-PEG-*b*-polyMTOS**—CTA-PEG<sub>8</sub> (1 equiv), SA (5 equiv) and DMAP (0.1 equiv) were dissolved in DMF (30 mL) anhydrous and added to a 50 mL round-bottom flask. Then, Et<sub>3</sub>N (10 equiv) was added dropwise with constant stirring using an ice bath under nitrogen atmosphere. The reaction mixture was kept under magnetic stirring for 24 h at room temperature (RT). At the end of the reaction, CTA-PEG<sub>8</sub>-COOH were dialysed (Spectrum Laboratories, 3.5 kDa MW cut-off) against distilled water for 72 h. The resulting solution was isolated by freeze-drying to yield white amorphous powders (yield >90%). The chemical structure of CTA-PEG<sub>8</sub>-COOH was confirmed by <sup>1</sup>H-NMR spectroscopy.

<sup>1</sup>H NMR spectrum (400 MHz, CDCl<sub>3</sub>): δ<sub>H</sub> 4.25 (t, *J* = 4.8 Hz, 4H), 3.63 (s, 860H), 3.31 (t, *J* = 7.4 Hz, 2H), 2.68–2.56 (m, 5H), 2.52 (m, 1H), 2.37 (m, 1H), 1.87 (s, 3H), 1.68 (quint, *J* = 7 Hz, 2H), 1.36 (quint, *J* = 7.6 Hz, 2H), 1.33–1.21 (m, 18H), 0.87 (t, *J* = 7 Hz, 3H) ppm.

COOH-PEG-*b*-poly(MTOS) was successfully synthesized by RAFT polymerization. CTA-PEG<sub>8</sub>-COOH, MTOS and AIBN were dissolved in anhydrous 1,4-dioxane and sealed in a 25 mL Schlenk tube. The total monomer concentration (M) and the feed molar ratio [MTOS]:[CTA]:[AIBN] were 0.5 M and [100]:[1]:[0.3], respectively. The reaction mixture was then degassed by three freeze-pump-thaw cycles and heated in an oil bath under magnetic stirring at 70 °C for 5 h. At the end of the polymerization, block copolymer was purified by dialysis (Spectrum Laboratories, 25 kDa MW cut-off) against a mixture of THF and EtOH (75:25 v:v) that was progressively replaced by water during three days. The polymer was finally isolated by freeze-drying (yield >90%) and its structure was confirmed by <sup>1</sup>H-NMR spectroscopy.

<sup>1</sup>H NMR spectrum (400 MHz, CDCl<sub>3</sub>): δ<sub>H</sub> 4.02–4.34 (2 × bs, 2H + 4H<sub>m</sub>), 3.64 (s, 4H + 4H<sub>n</sub>), 2.90–2.47 (3 × bs, 8H + 6H<sub>m</sub>), 2.10–1.88 (3 × s, 9H<sub>m</sub>), 1.84–0.94 (m, 23H + 28H<sub>m</sub>), 0.94–0.74 ppm (m, 3H + 12H<sub>m</sub>).

**Synthesis of IR-780-PEG-*b*-polyMTOS conjugate**—IR-780-NH was obtained as previously described[39]. Briefly, IR-780 iodide (1 equiv) and piperazine (5 equiv) were dissolved in 15 mL of dry DMF. The reaction mixture was then stirred and refluxed for 4 h at 80 °C. Afterwards, the solvent was removed under reduced pressure and the resulting product was purified by silica gel column chromatography using CH<sub>2</sub>Cl<sub>2</sub>/ EtOH (10:0.5, v/v) as eluent.

COOH-PEG-*b*-poly(MTOS) (1 equiv) was dissolved in THF anhydrous using a 50 mL round-bottom flask. IR-780-NH (5 equiv) and DMTMM (10 equiv) in DMF anhydrous were then added to a copolymer solution with constant stirring using an ice bath under nitrogen atmosphere. The reaction was stirred for 24 h under nitrogen atmosphere at RT. When the reaction time had elapsed, IR-780-PEG-*b*-poly(MTOS) conjugate were purified by dialysis (Spectrum Laboratories, 3.5 kDa MW cut-off) against a mixture of THF and EtOH (75:25 v:v) that was gradually replaced by distilled water over three days. The resulting solution was isolated by freeze-drying to yield green amorphous powder (yield 65%). The conjugation of the dye was confirmed by <sup>1</sup>H-NMR spectroscopy.

<sup>1</sup>H NMR spectrum (400 MHz, CDCl<sub>3</sub>): δ<sub>H</sub> 8.16 (d, *J* = 13.5 Hz, 2H), 7.37–7.27 (m, 2H), 6.90 (t, *J* = 7.4 Hz, 2H), 6.67 (d, *J* = 8.2 Hz, 2H), 5.46 (d, *J* = 13.5 Hz, 2H), 4.50–3.90 (2 × bs, 2H + 4H<sub>m</sub>), 3.85 (t, *J* = 5.1 Hz, 4H), 3.72 (t, *J* = 5.1 Hz, 4H), 3.64 (s, 4H + 4H<sub>n</sub>), 3.0–2.45 (3 × bs, 8H + 6H<sub>m</sub>), 2.10–1.85 (3 × s, 9H<sub>m</sub>), 1.84–0.94 (m, 23H + 28H<sub>m</sub>), 0.94–0.74 ppm (m, 3H + 12H<sub>m</sub>).

The chemical structure of the block copolymer and IR-780-based polymer conjugate were elucidated by <sup>1</sup>H-NMR spectroscopy in a Mercury 400BB apparatus, operating at 400 MHz. Additionally, the number and weight average molecular weight (*M<sub>n</sub>* and *M<sub>w</sub>*) and dispersity (*D*) of the block polymer were determined by size exclusion chromatography (SEC) using a Perkin-Elmer Isocratic LC pump 250 coupled to a refraction index detector (Series 200). Three polystyrene-divinyl benzene columns (Polymer Laboratories) of average pore size of 10<sup>3</sup>, 10<sup>4</sup> and 10<sup>5</sup> Å were used as solid phase, and degassed THF (1 mL/min) was used as eluent at 40°C. Monodisperse poly(methyl methacrylate) (PMMA) standards (Scharlab)

with MWs between 10.3 and 1400 kDa were used to obtain the calibration curve. Data were analyzed using the Perkin-Elmer LC solution program.

**Preparation of IR-780-based NPs**—Theranostic NPs were prepared by solvent exchange or SORP method. Specifically, 2 mL of 100 mM NaCl were incorporated dropwise over an organic dissolution (2 mL of THFMeOH or THF:EtOH 50:50 v:v) of IR-780-PEG-b-poly(MTOS) conjugate at 6 mg/mL under constant magnetic stirring. The final polymer concentration was 3 mg/mL. Additionally, IR-780 iodide (3, 5 and 10 % w/w with respect to polymer conjugate) was also incorporated to the organic phase with the aim to obtain NPs that entrapped this hydrophobic dye in their inner core. NP dispersions were dialyzed against 100 mM NaCl for 72 hours, followed by filtering through a 0.22 μM polyethersulfone membranes (PES, Millipore Express®, Millex GP).

### 2.3. Characterization of IR-780-based NPs

The particle size distribution and polydispersity (PDI) of NPs were determined by dynamic light scattering (DLS) using a Malvern Nanosizer NanoZS Instrument equipped with a 4 mW He-Ne laser ( $\lambda=633$  nm) at a scattering angle of 173°. All measurements were performed in square polystyrene cuvettes (SARSTEDT) at 25 °C. Additionally, zeta potential values were determined in NPs dispersions at 0.3 mg/mL, containing 10 mM NaCl, using laser Doppler electrophoresis (LDE) and the Smoluchowski's approximation. For each sample, the statistical average and standard deviation of data were calculated from 8 measurements of 20 runs each one.

IR-780 entrapped in the NPs was quantified by absorbance spectroscopy. Specifically, IR-NP-eIR (2 mg/mL) were dissolved in ethanol and their absorbance was measured with an excitation wavelength of 780 nm using a NanoDrop One UV-Vis Spectrophotometer. The absorbance was correlated with IR-780 concentration using a calibration curve that was previously obtained using a range of IR-780 concentrations between 0.1 – 0.001 mg/mL in ethanol. The encapsulation efficiency (EE) was defined as the ratio of calculated and original amount of IR-780 encapsulated in the NPs. The calculation equation is as follows:

$$\text{Encapsulation efficiency}(EE) = \frac{[\text{loaded molecule}]_i}{[\text{loaded molecules}]_0} \times 100 \quad [1]$$

Being  $[\text{loaded molecule}]_i$  the concentration of the molecule (IR-780) encapsulated in the inner core of the NPs and detected experimentally, and  $[\text{loaded molecule}]_0$  the concentration of the molecule added in the nanoprecipitation process.

The morphology of NPs was analyzed by scanning electron microscopy (SEM) using a Hitachi SU8000 TED, cold-emission FE-SEM microscope working with an accelerating voltage between 25 and 50 kV. Samples were prepared by deposition of one drop of the corresponding NP suspension (0.03 mg/mL) over small glass disks. The aqueous phase was evaporated at RT for 24 h. The samples were coated with gold palladium alloy (80:20) prior to examination by SEM.



The absorption and fluorescence properties of self-assembled NPs were measured using a Biotek SYNERGY-H4 microplate reader. The absorption spectra were obtained from 400-900 nm, while the emission spectra were recorded from 790 nm to 850 nm after excitation at 770 nm.

#### 2.4. Cell culture

Human mammary gland/breast carcinoma cells, MDA-MB-453 cells (ATCC HTB-131), derived from metastatic site, were cultured in Dulbecco's modified Eagle's medium (DMEM, Lonza), supplemented with 10% fetal bovine serum (FBS, Lonza) and 1% penicillin/streptomycin (Sigma).

#### 2.5. Cellular imaging studies

Uptake of IR-780-NPs by MDA-MB-453 cells was assessed by fluorescence microscopy.  $10^5$  MDA-MB-453 cells were seeded into 24 well-plates and incubated for 48 h at 37°C-5%CO<sub>2</sub>. Then, media were removed and cells were incubated at 37°C-5%CO<sub>2</sub> with fresh media containing NP dispersions at 1.5 mg/mL. After incubation for the indicated periods of time, cells were washed with cold PBS and fixed with 3.7 % (w/v) paraformaldehyde in PBS for 15 min at RT. Finally, cells were rinsed with cold PBS and visualized by fluorescence microscopy in the emission range of 825 nm, after excitation at 731 nm (EVOS® FL microscope). The fluorescence intensity was quantified using the ImageJ software. In some experiments, cells were observed by Confocal Laser Scanning Microscopy (CLSM, Leica TCS-SP5 RS AOBS), after excitation at 633 nm and collection of the emitted fluorescence in the range between 700 and 800 nm. In intracellular ROS assays, cells were observed by bright-field and epifluorescence microscopy. Fluorescence signal at 530 nm was collected after excitation at 480 nm using a Leica DM6000 B microscope.

#### 2.6. *In vitro* cytotoxicity assay

Cell viability was measured using the alamarBlue assay (Sigma-Aldrich)[40]. Briefly,  $6 \times 10^3$  MDA-MB-453 cells were seeded in 96-well plates. After 48 h of incubation at 37°C-5%CO<sub>2</sub>, medium was removed and cells were incubated with fresh media containing NP at 2.5-0.094 mg/mL for 24 h. After washing with PBS, samples were incubated in DMEM-10% FBS containing 10% (v/v) alamarBlue dye for 4 h at 37°C-5%CO<sub>2</sub>. After excitation at 530 nm, emitted fluorescence at 590 nm was quantified using a Synergy-HT spectrofluorimeter (Biotek).

#### 2.7. Photothermal and photodynamic behaviour of IR-780-based NPs

Suspensions containing different concentrations of IR-780-NP in NaCl (100 mM) were placed into polystyrene cuvettes and exposed to laser light of 808 nm emitting at 44 mW/mm<sup>2</sup>, using the experimental setup described elsewhere[41]. Temperature changes in NPs suspensions were monitored by IR thermography using a Testo 875-2i thermal imaging camera (Instrumentos Testo S.A.).

For NIR irradiation of cell cultures treated with NPs based in PEG-*b*-polyMTOS copolymer,  $1 \times 10^5$  MDA-MB-453 cells were seeded into a 48-well plate and incubated for 24 h at

37°C-5%CO<sub>2</sub>. Then, media were removed and cells were incubated further for 24 h with fresh media containing NPs at 0.375-0.094 mg/mL. After 24 h of incubation at 37°C-5%CO<sub>2</sub>, cells were washed with PBS and supplemented with fresh culture medium before irradiation with NIR-laser for 10 min inside a thermostatically-controlled chamber (Model Stuart SI60D, Fisher Scientific Afora) to establish the environmental temperature at 37 °C. In intracellular ROS assays, cells were treated with 100 μM 2',7'-Dichlorodihydrofluorescein diacetate (DCFH-DA, Cell Biolabs) for 1 h at 37°C-5%CO<sub>2</sub> and washed two times with PBS before laser irradiation. For intracellular 2',7'-Dichlorodihydrofluorescein (DCF) determination, cell extracts were obtained using Oxiselect lysis buffer (Cell Biolabs) following manufacturer's instructions. After excitation of cell extracts with 480 nm light, fluorescence at 530 nm was collected using Synergy4 spectrofluorimeter (Biotek). In phototoxicity assays, cell viability was measured using the alamarBlue assay as described in 3.6 Section.

## 2.8. Statistical analysis

Results were expressed as mean ± standard deviation (S.D.). Statistical significance (significance level of: \*: p < 0.05) was evaluated using the analysis of variance (ANOVA, Tukey test) as required, by Origin 9.

## 3. Results

### 3.1. Synthesis and characterization of IR-780-PEG-*b*-polyMTOS

Figure S1 (see supporting information) shows a schematic representation of the complete synthetic strategy that was used to obtain a IR-780-PEG-*b*-polyMTOS conjugate. CTA-PEG<sub>8</sub> was firstly modified to introduce carboxyl groups, yielding pure product after its purification. The chemical structure of CTA-PEG<sub>8</sub>-COOH was confirmed using <sup>1</sup>H-NMR spectroscopy by the appearance of the signals due to the characteristic protons of the methylene protons from the succinic anhydride at 2.6 ppm (CH<sub>2</sub>-h and CH<sub>2</sub>-i) (Figure 2). Other relevant characteristics of this macro-chain transfer agent (macro-CTA) are shown in Table 1. It is noteworthy that Đ was less than 1.20, confirming that the modification of the CTA allowed to maintain narrow molecular weight distribution of the hydrophilic CTA.

CTA-PEG<sub>8</sub>-COOH was successfully used to polymerize MTOS by RAFT at 70°C in anhydrous dioxane. <sup>1</sup>H-NMR spectra of the synthesized polymeric system COOH-PEG-*b*-poly(MTOS) is shown in Figure 3. Polymerization of the MTOS was confirmed by the broadening of the signals as a result of the macromolecular nature of the synthesized block polymers and the disappearance of the vinyl protons of MTOS. Furthermore, the appearance of new signals due to the methylene protons of the MTOS between 4.0 - 4.5 ppm (CH<sub>2</sub>- 2' and CH<sub>2</sub>-3') and 2.5-3.0 ppm (CH<sub>2</sub>- 5' and CH<sub>2</sub>-6') confirmed the presence of its chemical structure in the backbone of the copolymeric systems. Other characteristics proton signals of MTOS were appropriately assigned in the <sup>1</sup>H-NMR spectra of the synthesized copolymeric system (figure 3). After purification by dialysis, structural characteristics of synthesized block copolymer were determined (Table 1). The composition of the different block copolymers was elucidated by <sup>1</sup>H-NMR spectroscopy, using the methodology previously described by our group[27] (Figure 3). The MTOS molar composition into the copolymeric



system was 30 %-mol with a number average molecular weight higher than 65 kDa and low  $\bar{D}$  of 1.40 that confirming the good control of the polymerization, obtaining well-defined amphiphilic block copolymer.

Finally, IR-780-NH was successfully conjugated to the synthesized block copolymer by forming an amide bond between the amine group of the dye and the carboxyl group of PEG chains using DMTMM as coupling reagent[42]. The successful conjugation of the dye was confirmed by  $^1\text{H-NMR}$  spectroscopy by the appearance of the signals due to the aromatic protons of the dimethyl lindolinic ring between 6.5 and 7.5 ppm ( $\text{CH}_2\text{-1-4}$ ), the olefinic protons at 5.45 and 8.20 ppm ( $\text{CH}_2\text{-5}$  and  $\text{CH}_2\text{-6}$ ) and the protons from the piperazine functionalization at 3.72 and 3.85 ppm ( $\text{CH}_2\text{-a}$  and  $\text{CH}_2\text{-b}$ ) (figure 4).

### 3.2. Characterization of NPs based on IR-780-PEG-*b*-polyMTOS conjugate

IR-780-PEG-*b*-polyMTOS conjugate formed low polydispersed spherical NPs (Figure 5) by a spontaneous self-assembly process where PEG hydrophilic chains are most probably distributed in the external shell, stabilizing the MTOS-based hydrophobic core through inter- and intramolecular interactions. The most relevant characteristics of the NPs obtained from PEG-*b*-polyMTOS (unmodified-NP) and IR-780-PEG-*b*-polyMTOS conjugate are summarized in Table 2.

IR-NP exhibited an average hydrodynamic diameter of  $178.4 \pm 11.8$  nm when a mixture THF:MeOH (50:50 v:v) was used during the precipitation by solvent exchange. However, the replacement of MeOH by EtOH allowed obtaining IR-NP of reduced size and PDI (Figure 5A). Additionally, IR-NP dispersions had zeta potential values around +3 mV. Finally, SEM microscopy was used to confirm the uniformity of the monodisperse suspension of spherical IR-NP (Figure 5B).

**3.3. Self-assembled IR-NP with additional load of IR-780 iodide in their inner core were appointed as a function of the feed percentage of IR-780 iodide entrapped: IR-NP-eIR3, IR-NP-eIR5 and IR-NP-eIR10 for 3, 5 or 10 % w/w with respect to polymer conjugate, respectively. As it is shown in Table 2, particle size, PDI and zeta potential values increased with the amount of IR-780 iodide loaded. In all cases, IR-780 was efficiently entrapped in the core of the NPs with EE higher than 85 %. **Optical properties of NPs based on IR-780-PEG-*b*-polyMTOS conjugate****

Formation of self-assembling NPs significantly affected the optical properties of the NIR dye conjugated to COOH-PEG-*b*-polyMTOS. Polymeric conjugate exhibited a maximum emission peak around 810 nm (Figure 6A). Emission intensity of the polymer conjugate changed when self-assembled by SORP in aqueous media and eliminated the organic solvent by dialysis. Photostability during storage of IR-NP in aqueous media was confirmed, being NIR fluorescence constant during, at least, 1 week of incubation at 37 °C (Figure 6B).

Encapsulation of additional IR-780 iodide in the inner core of IR-NP significantly modified their optical properties. Emission spectra after NIR excitation (Figure 6C-D) revealed a severe quenching of emitted fluorescence in IR-NP-eIR5.

IR-NP-eIR5 was selected for the following experiments as a compromise was reached in terms of hydrodynamic diameter, optical and photoresponsive properties.

### 3.4. Cellular internalization of IR-780-based NPs

3.5. Uptake of IR-NP by tumor cells was studied exploiting the NIR-fluorescence properties of the IR-780 dye. MDA-MB-453 cells were exposed to IR-NP and monitored at different time points along 8 h of incubation at 37°C (Figure 7A). Fluorescence measurements in the NIR range demonstrated that fluorescence intensity detected in the cell culture increased gradually with time of exposure to IR-NP. CLSM images of cells treated with IR-NP for 5 h showed that IR-780 dye was distributed in the cytoplasm around the nucleus (Figure 7B).

#### Cell toxicity of IR-780-based NPs

The cytotoxic activity of unmodified-NP, IR-NP or IR-NP-eIR in MDA-MB-453 cells was studied after 24 h of treatment. As shown in Figure 8, 2.5 mg/mL of unmodified-NP reduced by 35 % the metabolic activity of cell culture while 0.188 mg/mL of IR-NP or IR-NP-eIR5 was sufficient to reduce cell viability to levels below 70%. It is noteworthy that the encapsulation of additional IR-780 dye in the core of IR-NP increased significantly the cytotoxicity of the nanomaterial when it was used at concentrations 0.375 mg/mL.

### 3.6. Photothermal properties of IR-780-based NPs

The photothermal properties of IR-NP and IR-NP-eIR5 were investigated in aqueous solutions that were irradiated using a NIR laser emitting at 808 nm. As control, unmodified-NPs were subjected to same NIR treatment. Analysis of infrared thermal images revealed that irradiation of 0.375 mg/mL IR-NP for 5 min only increased the temperature of the medium by about 2 °C (Figure 9B). This temperature rise, that slightly exceeded the heating level occurring in the sample by laser scattering and minimum NIR energy absorption in the aqueous media, could not be detected in suspensions containing 0.375 mg/mL of unmodified-NPs (Figure 9A) or lower concentrations of IR-NP. Thermal curves obtained by IR thermography of IR-NP-eIR5 suspensions showed a rapid and substantial increase in the temperature of the samples during the first 2 min of NIR-irradiation that gradually reached a steady level (Fig. 9C). NIR irradiation of suspensions containing 0.375 mg/mL IR-NP-eIR5 led to an average net temperature increase of about 21 °C higher than that detected due to unspecific heating of the sample. A dose-dependent increase of temperature could be clearly observed in NIR-irradiated suspensions containing IR-NP-eIR5.

### 3.7. Phototoxicity of NPs based on IR-780-PEG-*b*-polyMTOS conjugate

In order to investigate the photothermal toxicity of NPs based on IR-780-PEG-*b*-polyMTOS conjugate, MDA-MB-453 cells were incubated with IR-NP or IR-NP-eIR5 for 24 h and then irradiated with 808 nm NIR laser for 10 minutes. Metabolic activity measurements in MBA-MD-453 cells after 18 h of the NIR treatment are summarized in Figure 10. Metabolic activity of NP-untreated cells did not significantly change after NIR irradiation. Increasing concentration of unmodified-NP did not alter significantly the metabolic activity after NIR irradiation, which was similar to that detected in cell cultures not exposed to NPs (Fig 10A). Laser treatment of cells preincubated with NPs reduced their metabolic activity in a dose-dependent manner. Thus, 0.094 mg/mL IR-NP was sufficient to reduce by more than 60%

the viability of NIR-irradiated cultures (Figure 10B), while illumination of cells treated with 0.375 mg/mL resulted in negligible metabolic activity (< 0.6%) relative to control. MDA-MB-453 cells, preincubated with same concentration range of IR-NP-eIR5, showed a marked decline in viability which was reinforced by the NIR-laser treatment to achieve metabolic activity levels similar to those found in cells exposed to IR-NP and NIR-light (figure 10C). Increasing concentration of unmodified-NP did not alter significantly the metabolic activity after NIR irradiation, which was similar to that detected in cell cultures not exposed to NPs.

To assess the cytotoxicity of byproducts derived from the irradiation of IR-780-PEG-*b*-polyMTOS nanoassemblies, unmodified-NPs or IR-NP suspensions were irradiated with the NIR laser for 10 min and then immediately added to cultures of MBA-MD-453 cells. Laser treatment of IR-NP promoted a noticeable photobleaching of IR-780 (Figure 11A) and reduced the cytotoxic activity of the nanoassemblies suspension (Figure 11B, right panel). Metabolic activity of cell cultures was not affected after treatment with illuminated suspension of unmodified-NPs (Figure 11B, left panel). Altogether, these results suggested that cytotoxicity exerted by IR-NP depends on the integrity of IR-780 dye.

Finally, we studied whether the phototoxicity exhibited by IR-NP could be due to a photodynamic activity induced by the NIR-laser. Irradiated MDA-MB-453 cells, preincubated with IR-NP and loaded with the fluorogenic probe DCFH-DA, accumulated large amounts of DCF, the oxidized form of the compound. This phenomenon could not be observed in cells preincubated with unmodified-NP (Figure 12). This assay, based on the correlation between the fluorescence intensity emitted by the oxidized fluorogenic probe and the ROS levels within cell cytosol, demonstrated that IR-NP at photothermally inefficient concentrations can notably unbalance the cellular oxidative status after NIR irradiation.

#### 4- Discussion

To overcome the low solubility of  $\alpha$ -TOS in physiological media, PEG-*b*-polyMTOS with different PEG:MTOS ratios were successfully synthesized by RAFT polymerization. These bioactive block copolymers present the ability to self-assemble in aqueous media forming micellar nanoaggregates with a hydrophilic shell and a hydrophobic core capable of encapsulating and transport other hydrophobic molecules. Due to its high MTOS content, PEG-*b*-polyMTOS (71:29) exhibited significant cytotoxic activity [27].

The easy functionalization of PEG hydroxyl end group facilitates the incorporation of therapeutic agents in PEG-*b*-polyMTOS. <sup>1</sup>H-NMR spectroscopy demonstrated the incorporation of the carboxylic group by the appearance of the methylene protons CH<sub>2</sub>-f at 4.25 ppm, and CH<sub>2</sub>-h or CH<sub>2</sub>-i protons within range between 2.30 and 2.70 ppm (Figure 2). SEC characterization of this CTA confirmed that the incorporation of carboxyl groups maintained its narrow MW distribution with a *D* value of 1.12 (Table 1). Polymerization of the MTOS under RAFT controlled conditions using CTA-PEG<sub>8</sub>-COOH was confirmed by the disappearance of the vinyl protons of MTOS between 5.5 and 6.5 ppm, the appearance of its characteristics proton signals and the broadening of the signals as a result of the macromolecular nature of the synthesized block polymers. According to <sup>1</sup>H-NMR

spectroscopy, COOH-PEG-*b*-poly(MTOS) with a molar composition of PEGMTOS 70:30 was obtained. Additionally, SEC characterization indicated that polymeric system presented a MW higher than 65 kDa with a relatively low  $\mathcal{D}$  as a result of the control over the polymerization.

IR-780-NH was conjugated to the block copolymer using DMTMM as coupling reagent due to its several advantages in comparison to other reagents as EDC. In particular, DMTMM is a triazine derivative that facilitates an efficient one-step condensation of polymers and other small molecules with a high yield, easy removal of subproducts and a wide range of reaction conditions regarding to the use of solvents or pH range [39-41]. As it is shown in Figure 4, the conjugate spectrum contained peaks contributed by IR-780 dye and the polymeric system based in PEG.

Size and PDI of IR-NP were significantly reduced by changing the organic phase during SORP probably due to the improved solubility of the polymeric conjugate in the THF:EtOH (50:50) mixture. The positive zeta potential demonstrated the presence of the IR-780 lipophilic cation in the external shell of the NPs. The positive charge of NPs incorporating IR-780 dye has been described by other authors. In this sense, Yuan *et al.* conjugated IR-780 iodide to the chemical structure of PEG<sub>2000</sub>, obtaining micelles with a zeta potential around +8 mV [22]. Self-assembled IR-NP with additional load of IR-780 iodide in their inner core were successfully synthesized in order to combine the chemical conjugation and the physical entrapment of the NIR-dye in a single nanotheranostics platform. Although particle size, PDI and zeta potential values increased with the amount of IR-780 iodide loaded,  $D_h$  of IR-NP-eIR remained below 170 nm. Very recently, Pais-Silva *et al.* successfully encapsulated IR-780 in the inner core of NPs based on  $\beta$ - $\alpha$ -tocopheryl polyethylene glycol succinate (TPGS) and  $\alpha$ -TOS. However, these authors did not investigate the chemical conjugation of the dye and its incorporation into NPs with controlled molecular architecture [43].

Intensity of NIR fluorescence emission decreased after incorporation of aqueous media by SORP and purification of NPs by dialysis, probably because the hydrophilic media significantly screened off the fluorescence of IR-780. The emission intensity of IR-NP-eIR compared to IR-NP was severely quenched by the self-aggregation of the dye, most likely due to a significant energy transfer between the dye molecules. In fact, Shimizu *et al.* successfully entrapped the cyanine dye IC7-1 in the core of amphiphilic lactosomes based on poly(sarcosine)-*b*-poly(L-lactate). These authors demonstrated that the IC7-1 NIR-fluorescence was quenched with increasing concentrations of the NIR-dye entrapped into the lactosomes [20].

Data showed in Figure 7B suggest that IR-NP rapidly incorporate in cancer cells, allowing sustained real-time monitoring by imaging techniques. According to the literature, the majority of NPs with sizes between 100 and 200 nm enter into cells via endocytosis pathways and accumulate within intracellular vesicles [44]. This process is strongly influenced by the surface charge of the nanomaterial. As previously mentioned, IR-NP and IR-NP-eIR had positive surface charge as a result of the cationic nature of the lipophilic dye. For this reason, the cellular uptake of these NPs and their affinity for the mitochondria could be favored in tumor cells due to the hyperpolarization of cell and mitochondria membranes

[32, 45-49]. Furthermore, additional mechanisms may contribute to favored cellular uptake of NPs incorporating IR-780. In this sense, Yang *et al.* have exhaustively investigated the influence of organic anion transporter peptides (OATPs) that are overexpressed in various types of cancer cells [48]. These authors demonstrated that cellular uptake of heptamethine cyanine dyes could be mediated by these peptides since its internalization was prevented by the addition of OATPs inhibitors such as bromosulfophthalein (BSP) [50].

Encapsulation of additional amounts of NIR-probe into the hydrophobic core of IR-780-PEG-*b*-polyMTOS nanoassemblies intensified their cytotoxic character (Figure 8) and changed markedly their photothermal behavior as recently described by Zhu et al.[51] that encapsulated indocyanine green dye in polymeric vesicles to obtain NIR fluorescent NP with synergized thermo-chemotherapeutic properties.

For the range of tested doses, IR-NPeIR5 was very efficient at transducing NIR-energy into heat, most likely due the spatial confinement of high amounts of NIR-probe inside the nanoassembly [12]. Contrarily, aqueous solutions of IR-NP showed a very poor ability to dissipate heat to the environment after the exposure to incident NIR-light. Hence, other mechanisms different to hyperthermia may be responsible of the cytotoxicity enhancement observed after NIR-laser irradiation of cells incorporating IR-NP (Figure 9). We hypothesized that NIR irradiation of IR-NP may result in byproducts with higher cytotoxic potential than the NIR dye. However, data shown in Figure 10 did not support this hypothesis as cytotoxicity of IR-NP suspension was drastically reduced after illumination with the NIR-laser. This finding may be explained by the severe photobleaching observed in irradiated IR-NP suspensions (Figure 11A), indicating that cytotoxic activity of the nanoassemblies depends largely on the persistence of intact IR-780 dye.

We then hypothesized that IR-NP phototoxicity, which does not depend on cell heating, might be due to a photodynamic activity conducted by the NIR-dye acting as a photosensitizer. Thereby, the photochemical reactions triggered by the photoactivation of the probe may involve the generation of ROS with a short lifetime that immediately reacts with nearby biomolecules and causes the damage of cell structures [11, 52, 53]. In this sense, Jiang *et al.* investigated the phototherapeutic effect of IR-780 encapsulated in the core of biodegradable human serum albumin NPs (HSA-NP). These authors observed that NIR-irradiation of IR-780-HAS-NP resulted in a simultaneous increase of temperature and high amount of ROS species [17]. Data shown in Figure 12 demonstrate that NIR-irradiation resulted in the induction of intracellular ROS in MDA-MB-453 cells incubated with IR-NP. This phenomenon could not be observed in cells treated with PEG-*b*-polyMTOS nanoassemblies devoid of IR-780, suggesting that oxidative stress mechanisms, independent of heat generation, underlie the phototoxicity induced by IR-NP. This phenomenon was also observed by Pais-Silva with IR-780-loaded micelles based on TPGS and  $\alpha$ -TOS. Although the heat generation of the NP suspension was not efficient (temperature increment of 2°C), the intracellular concentration of ROS increased considerably when the suspension was laser irradiated at 808 nm (1.7 W cm<sup>-2</sup>, 5 minutes)[43].

High sensitivity of malignant cells to  $\alpha$ -TOS effects is based on its ability to efficiently induce the mitochondrial signal transmissions mechanisms, including ROS generation,

which trigger apoptosis [54]. Previous studies concluded that propensity for cells to accumulate ROS is a prerequisite before they can be killed by  $\alpha$ -TOS [52], explaining at least partially the selectivity of vitamin E analogues for cancer cells [53]. This hypothesis is consistent with the fact that cancer cells commonly express lower levels of anti-oxidant enzymes, such as the manganese superoxide dismutase (MnSOD) [55], than normal cells which are thus protected against  $\alpha$ -TOS toxicity through mechanisms that hinder ROS accumulation [53]. Future work will focus on elucidating whether  $\alpha$ -TOS derivative constituent of the amphiphilic block copolymer used in this work interacts with IR-780, resulting in enhancement of cytotoxicity upon NIR irradiation. The extension of the proposed study to the *in vivo* scenario will evaluate the clinical potential of the developed nanotheranostic platform in antitumor applications.

#### 4. Conclusions

IR-780 dye was conjugated to PEG-*b*-polyMTOS copolymer to obtain NIR-fluorescent NPs by SORP occurring in aqueous medium. These NPs were efficiently internalized by MBA-MD-453 and showed cytotoxic activity. During the self-assembly of IR-NP, physical encapsulation of additional IR-780 was possible by the hydrophobic core resulting in the generation of IR-NP-eIR with a modulable content in NIR-probe. NIR-fluorescence exhibited by IR-NP-eIR was severely quenched by their cargo, but their photothermal behavior was much higher than that exhibited by IR-NP. However, NIR-irradiation of cancer cells preincubated with IR-NP resulted in a dramatic reduction of their metabolic activity. The inducible phototoxicity conducted by IR-NP could not be attributed to the generation of lethal heating or cytotoxic byproducts originated from the photodegradation of IR780-PEG-*b*-polyMTOS copolymer. We demonstrated that NIR-illumination of malignant cells treated with IR-NP resulted in a remarkable imbalance of intracellular ROS, and therefore, a disturbance in the oxidative status which leads to cell death.

#### Supplementary Material

Refer to Web version on PubMed Central for supplementary material.

#### Acknowledgments

Authors would like to thank financial support from the Spanish Ministry of Economy and Competitiveness (MAT2014-51918-C2-1-R and SAF2013-50364-EXP), CIBER BBN-ECO Foundation project, Instituto Salud Carlos III (ISCIII)-Fondos FEDER, MINECO-AES (PI15/01118), CSIC (201660I028), and the National Institutes of Health Cell and Tissue Engineering Training Grant T32 GM008433. Authors also acknowledge, David Gómez, Rosa Ana Ramírez and Mar Fernández and María Isabel Trabado for their help in SEM, cell culture and CLSM experiments, respectively.

#### References

1. Muthu MS, Leong DT, Mei L, Feng SS. Nanotheranostics- application and further development of nanomedicine strategies for advanced theranostics. *Theranostics*. 2014; 4:660–7. [PubMed: 24723986]
2. Thakor AS, Gambhir SS. Nanooncology: the future of cancer diagnosis and therapy. *CA: a cancer journal for clinicians*. 2013; 63:395–418. [PubMed: 24114523]
3. Ahmed N, Fessi H, Elaissari A. Theranostic applications of nanoparticles in cancer. *Drug Discovery Today*. 2012; 17:928–34. [PubMed: 22484464]



4. Mukerjee A, P Ranjan A, K Vishwanatha J. Combinatorial nanoparticles for cancer diagnosis and therapy. *Current medicinal chemistry*. 2012; 19:3714–21. [PubMed: 22680922]
5. Barlas FB, Demir B, Guler E, Senisik AM, Arican HA, Unak P, Timur S. Multimodal theranostic assemblies: double encapsulation of protoporphyrine-IX/Gd 3+ in niosomes. *RSC Advances*. 2016; 6:30217–25.
6. Xie J, Lee S, Chen X. Nanoparticle-based theranostic agents. *Advanced drug delivery reviews*. 2010; 62:1064–79. [PubMed: 20691229]
7. Issels RD. Hyperthermia adds to chemotherapy. *European Journal of Cancer*. 2008; 44:2546–54. [PubMed: 18789678]
8. Mroz P, Yaroslavsky A, Kharkwal GB, Hamblin MR. Cell death pathways in photodynamic therapy of cancer. *Cancers*. 2011; 3:2516–39. [PubMed: 23914299]
9. Dolmans DE, Fukumura D, Jain RK. Photodynamic therapy for cancer. *Nature reviews cancer*. 2003; 3:380–7. [PubMed: 12724736]
10. Tan X, Luo S, Wang D, Su Y, Cheng T, Shi C. A NIR heptamethine dye with intrinsic cancer targeting, imaging and photosensitizing properties. *Biomaterials*. 2012; 33:2230–9. [PubMed: 22182749]
11. Shibu ES, Hamada M, Murase N, Biju V. Nanomaterials formulations for photothermal and photodynamic therapy of cancer. *Journal of Photochemistry and Photobiology C: Photochemistry Reviews*. 2013; 15:53–72.
12. Yuan A, Wu J, Tang X, Zhao L, Xu F, Hu Y. Application of near-infrared dyes for tumor imaging, photothermal, and photodynamic therapies. *Journal of pharmaceutical sciences*. 2013; 102:6–28. [PubMed: 23132644]
13. Song X, Chen Q, Liu Z. Recent advances in the development of organic photothermal nano-agents. *Nano Research*. 2015; 8:340–54.
14. Luo S, Zhang E, Su Y, Cheng T, Shi C. A review of NIR dyes in cancer targeting and imaging. *Biomaterials*. 2011; 32:7127–38. [PubMed: 21724249]
15. Resch-Genger U, Grabolle M, Cavaliere-Jaricot S, Nitschke R, Nann T. Quantum dots versus organic dyes as fluorescent labels. *Nat Methods*. 2008; 5:763–75. [PubMed: 18756197]
16. Conceição DS, Ferreira DP, Ferreira LFV. Photochemistry and Cytotoxicity Evaluation of Heptamethinecyanine Near Infrared (NIR) Dyes. *International journal of molecular sciences*. 2013; 14:18557–71. [PubMed: 24022690]
17. Jiang C, Cheng H, Yuan A, Tang X, Wu J, Hu Y. Hydrophobic IR780 encapsulated in biodegradable human serum albumin nanoparticles for photothermal and photodynamic therapy. *Acta biomaterialia*. 2015; 14:61–9. [PubMed: 25463484]
18. Peng CL, Shih YH, Lee PC, Hsieh TMH, Luo TY, Shieh MJ. Multimodal image-guided photothermal therapy mediated by 188Re-labeled micelles containing a cyanine-type photosensitizer. *ACS nano*. 2011; 5:5594–607. [PubMed: 21671580]
19. Singh AK, Hahn MA, Gutwein LG, Rule MC, Knapik JA, Moudgil BM, Grobmyer SR, Brown SC. Multi-dye theranostic nanoparticle platform for bioimaging and cancer therapy. *International journal of nanomedicine*. 2012; 7:2739. [PubMed: 22701319]
20. Shimizu Y, Temma T, Hara I, Makino A, Yamahara R, Ozeki Ei, Ono M, Saji H. Micelle-based activatable probe for in vivo near-infrared optical imaging of cancer biomolecules. *Nanomedicine: Nanotechnology, Biology and Medicine*. 2014; 10:187–95.
21. Yue C, Liu P, Zheng M, Zhao P, Wang Y, Ma Y, Cai L. IR-780 dye loaded tumor targeting theranostic nanoparticles for NIR imaging and photothermal therapy. *Biomaterials*. 2013; 34:6853–61. [PubMed: 23777910]
22. Yuan A, Qiu X, Tang X, Liu W, Wu J, Hu Y. Self-assembled PEG-IR-780-C13 micelle as a targeting, safe and highly-effective photothermal agent for in vivo imaging and cancer therapy. *Biomaterials*. 2015; 51:184–93. [PubMed: 25771009]
23. Maeda H, Nakamura H, Fang J. The EPR effect for macromolecular drug delivery to solid tumors: Improvement of tumor uptake, lowering of systemic toxicity, and distinct tumor imaging in vivo. *Advanced drug delivery reviews*. 2013; 65:71–9. [PubMed: 23088862]
24. Veronese FM, Pasut G. PEGylation, successful approach to drug delivery. *Drug discovery today*. 2005; 10:1451–8. [PubMed: 16243265]

25. Jokerst JV, Lobovkina T, Zare RN, Gambhir SS. Nanoparticle PEGylation for imaging and therapy. *Nanomedicine*. 2011; 6:715–28. [PubMed: 21718180]
26. York AW, Kirkland SE, McCormick CL. Advances in the synthesis of amphiphilic block copolymers via RAFT polymerization: stimuli-responsive drug and gene delivery. *Advanced drug delivery reviews*. 2008; 60:1018–36. [PubMed: 18403044]
27. Palao-Suay R, Aguilar MR, Parra-Ruiz FJ, Maji S, Hoogenboom R, Rohner N, Thomas SN, San Román J.  $\alpha$ -TOS-based RAFT block copolymers and their NPs for the treatment of cancer. *Polymer Chemistry*. 2016; 7:838–50. [PubMed: 27004068]
28. Dong LF, Neuzil J. Mitochondria in Cancer: Why Mitochondria Are a Good Target for Cancer Therapy. *Progress in molecular biology and translational science*. 2014; 127:211. [PubMed: 25149219]
29. Dong LF, Jameson VJ, Tilly D, Cerny J, Mahdavian E, Marín-Hernández A, Hernández-Esquivel L, Rodríguez-Enríquez S, Stursa J, Witting PK. Mitochondrial targeting of vitamin E succinate enhances its pro-apoptotic and anti-cancer activity via mitochondrial complex II. *Journal of Biological Chemistry*. 2011; 286:3717–28. [PubMed: 21059645]
30. Wang XF, Birringer M, Dong LF, Veprek P, Low P, Swettenham E, Stantic M, Yuan LH, Zobalova R, Wu K. A peptide conjugate of vitamin E succinate targets breast cancer cells with high ErbB2 expression. *Cancer Research*. 2007; 67:3337–44. [PubMed: 17409443]
31. Palao-Suay R, Rodríguez L, Aguilar MR, Sánchez-Rodríguez C, Parra F, Fernández M, Parra J, Riestra-Ayora J, Sanz-Fernández R, Román JS. Mitochondrially Targeted Nanoparticles Based on  $\alpha$ -TOS for the Selective Cancer Treatment. *Macromolecular Bioscience*. 2015
32. Murphy MP. Targeting lipophilic cations to mitochondria. *Biochimica et Biophysica Acta (BBA)-Bioenergetics*. 2008; 1777:1028–31. [PubMed: 18439417]
33. Fulda S, Galluzzi L, Kroemer G. Targeting mitochondria for cancer therapy. *Nature reviews Drug discovery*. 2010; 9:447–64. [PubMed: 20467424]
34. Davis S, Weiss M, Wong J, Lampidis TJ, Chen LB. Mitochondrial and plasma membrane potentials cause unusual accumulation and retention of rhodamine 123 by human breast adenocarcinoma-derived MCF-7 cells. *Journal of Biological Chemistry*. 1985; 260:13844–50. [PubMed: 4055760]
35. Chen LB. Mitochondrial membrane potential in living cells. *Annual review of cell biology*. 1988; 4:155–81.
36. Zhang E, Luo S, Tan X, Shi C. Mechanistic study of IR-780 dye as a potential tumor targeting and drug delivery agent. *Biomaterials*. 2014; 35:771–8. [PubMed: 24148240]
37. Wang Y, Liu T, Zhang E, Luo S, Tan X, Shi C. Preferential accumulation of the near infrared heptamethine dye IR-780 in the mitochondria of drug-resistant lung cancer cells. *Biomaterials*. 2014; 35:4116–24. [PubMed: 24529902]
38. Palao-Suay R, Aguilar MR, Parra-Ruiz FJ, Fernández-Gutiérrez M, Parra J, Sánchez-Rodríguez C, Sanz-Fernández R, Rodríguez L, Román JS. Anticancer and Antiangiogenic Activity of Surfactant-Free Nanoparticles Based on Self-Assembled Polymeric Derivatives of Vitamin E: Structure–Activity Relationship. *Biomacromolecules*. 2015; 16:1566–81. [PubMed: 25848887]
39. Li CY, Kong XF, Li YF, Zou CX, Liu D, Zhu WG. Ratiometric and colorimetric fluorescent chemosensor for Ag<sup>+</sup> based on tricarbocyanine. *Dyes and Pigments*. 2013; 99:903–7.
40. Page B, Page M, Noel C. A new fluorometric assay for cytotoxicity measurements in vitro. *Int J Oncol*. 1993; 3:473–6. [PubMed: 21573387]
41. Cebrián V, Martín-Saavedra F, Gómez L, Arruebo M, Santamaria J, Vilaboa N. Enhancing of plasmonic photothermal therapy through heat-inducible transgene activity. *Nanomed Nanotechnol Biol Med*. 2013; 9:646–56.
42. Reyes-Ortega F, Parra-Ruiz FJ, Averick SE, Rodríguez G, Aguilar MR, Matyjaszewski K, San Román J. Smart heparin-based bioconjugates synthesized by a combination of ATRP and click chemistry. *Polymer Chemistry*. 2013; 4:2800–14.
43. Pais-Silva C, de Melo-Diogo D, Correia IJ. IR780-loaded TPGS-TOS micelles for breast cancer photodynamic therapy. *European Journal of Pharmaceutics and Biopharmaceutics*. 2017; 113:108–17. [PubMed: 28087376]

44. Yameen B, Choi WI, Vilos C, Swami A, Shi J, Farokhzad OC. Insight into nanoparticle cellular uptake and intracellular targeting. *Journal of Controlled Release*. 2014; 190:485–99. [PubMed: 24984011]
45. Marquez M, Nilsson S, Lennartsson L, Liu Z, Tammela T, Raitanen M, Holmberg A. Charge-dependent targeting: results in six tumor cell lines. *Anticancer research*. 2004; 24:1347–52. [PubMed: 15274294]
46. Ross MF, Da Ros T, Blaikie FH, Prime TA, Porteous CM, Severina II, Skulachev VP, Kjaergaard HG, Smith RA, Murphy MP. Accumulation of lipophilic dications by mitochondria and cells. *Biochemical journal*. 2006; 400:199–208. [PubMed: 16948637]
47. Rin Jean S, Tulumello DV, Wisnovsky SP, Lei EK, Pereira MP, Kelley SO. Molecular vehicles for mitochondrial chemical biology and drug delivery. *ACS chemical biology*. 2014; 9:323–33. [PubMed: 24410267]
48. Smith RA, Porteous CM, Gane AM, Murphy MP. Delivery of bioactive molecules to mitochondria in vivo. *Proceedings of the National Academy of Sciences*. 2003; 100:5407–12.
49. Dolowy K. Bioelectrochemistry of cell surfaces. *Prog Surf Sci*. 1984; 15:245–368.
50. Yang X, Shi C, Tong R, Qian W, Zhou HE, Wang R, Zhu G, Cheng J, Yang VW, Cheng T. Near IR heptamethine cyanine dye-mediated cancer imaging. *Clinical Cancer Research*. 2010; 16:2833–44. [PubMed: 20410058]
51. Zhu A, Miao K, Deng Y, Ke H, He H, Yang T, Guo M, Li Y, Guo Z, Wang Y, Yang X, Zhao Y, Chen H. Dually pH/Reduction-Responsive Vesicles for Ultrahigh-Contrast Fluorescence Imaging and Thermo-Chemotherapy-Synergized Tumor Ablation. *ACS Nano*. 2015; 9:7874–85. [PubMed: 26181349]
52. Lucky SS, Soo KC, Zhang Y. Nanoparticles in photodynamic therapy. *Chemical reviews*. 2015; 115:1990–2042. [PubMed: 25602130]
53. Nguyen KT, Menon JU, Jadeja PV, Tambe PP, Vu K, Yuan B. Nanomaterials for photo-based diagnostic and therapeutic applications. *Theranostics*. 2013; 3:152–66. [PubMed: 23471164]
54. Weber T, Dalen H, Andera L, Nègre-Salvayre A, Augé N, Sticha M, Lloret A, Terman A, Witting PK, Higuchi M, Plasilova M, Zivny J, Gellert N, Weber C, Neuzil J. Mitochondria play a central role in apoptosis induced by  $\alpha$ -tocopheryl succinate, an agent with antineoplastic activity: Comparison with receptor-mediated pro-apoptotic signaling. *Biochemistry*. 2003; 42:4277–91. [PubMed: 12680782]
55. Borrello S, De Leo M, Galeotti T. Defective gene expression of MnSOD in cancer cells. *Mol Aspects Med*. 1993; 14:253–8. [PubMed: 8264340]

### State of significance

Multifunctional polymeric nanoparticles (NPs) that combine imaging and therapeutic properties are highly valuable in cancer treatment. In this paper we describe the development of NPs that are fluorescent in the near-infrared (NIR). This is important for their visualization in living tissues that present low absorption and low autofluorescence in this wavelength region (between 700 and 1000 nm). Moreover, NPs present photothermal and photodynamic properties when NIR irradiated: the NPs produce an efficient increment of temperature and increase the intracellular reactive oxygen species (ROS) when laser irradiated at 808 nm. These tuneable photoinduced properties make the NPs highly cytotoxic after NIR irradiation and provides a new tool for highly precise cancer treatment.

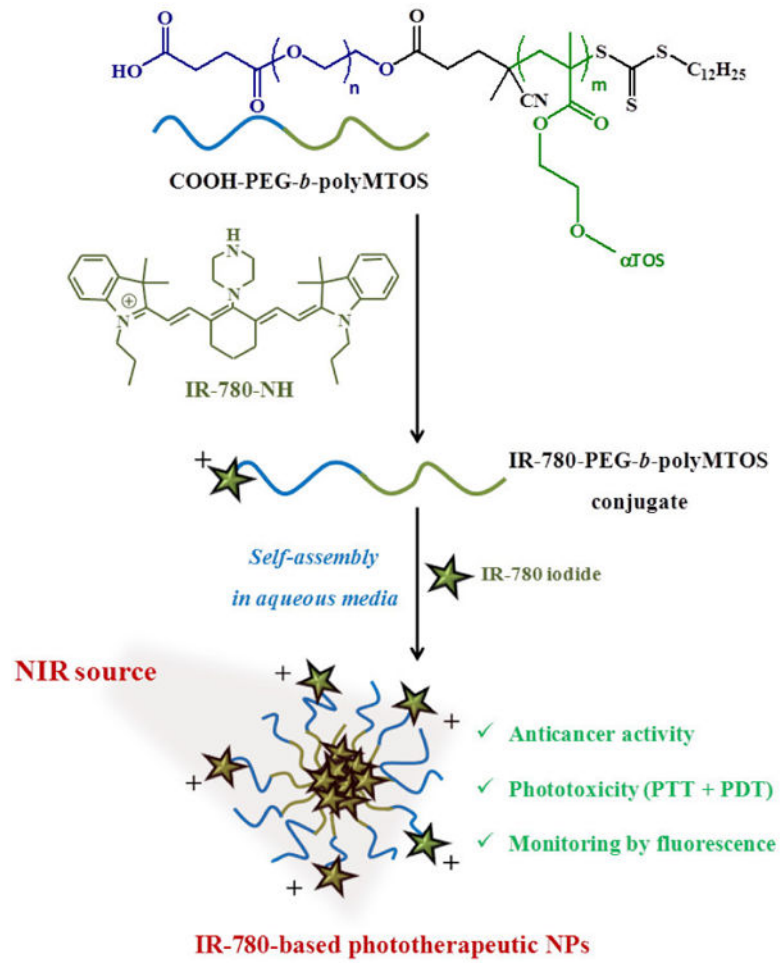


Figure 1. Scheme of preparation of IR-780-based NPs

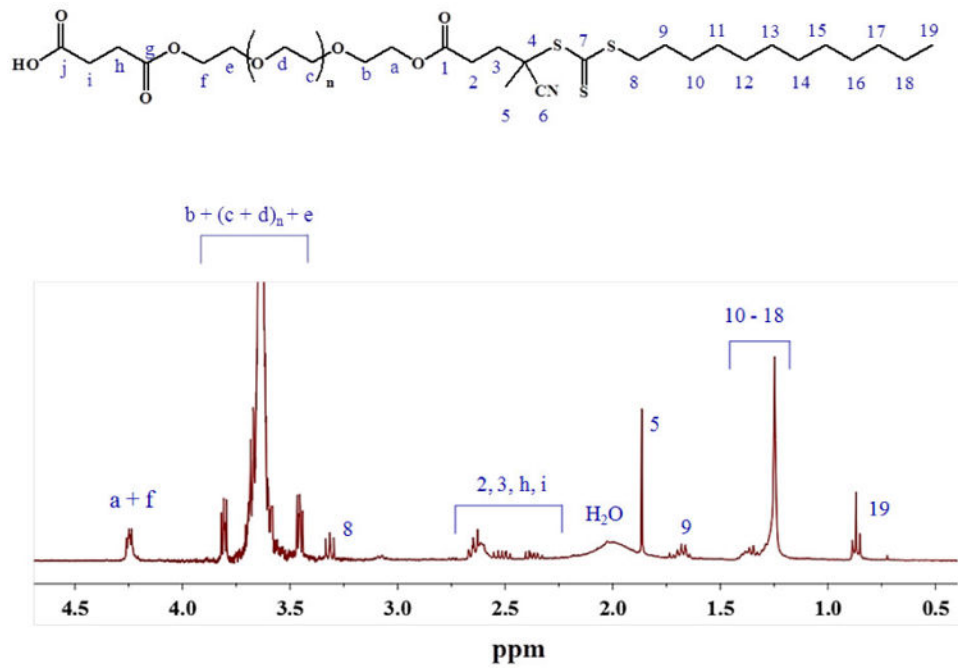


Figure 2. <sup>1</sup>H-NMR spectra of CTA-PEG<sub>8</sub>-COOH



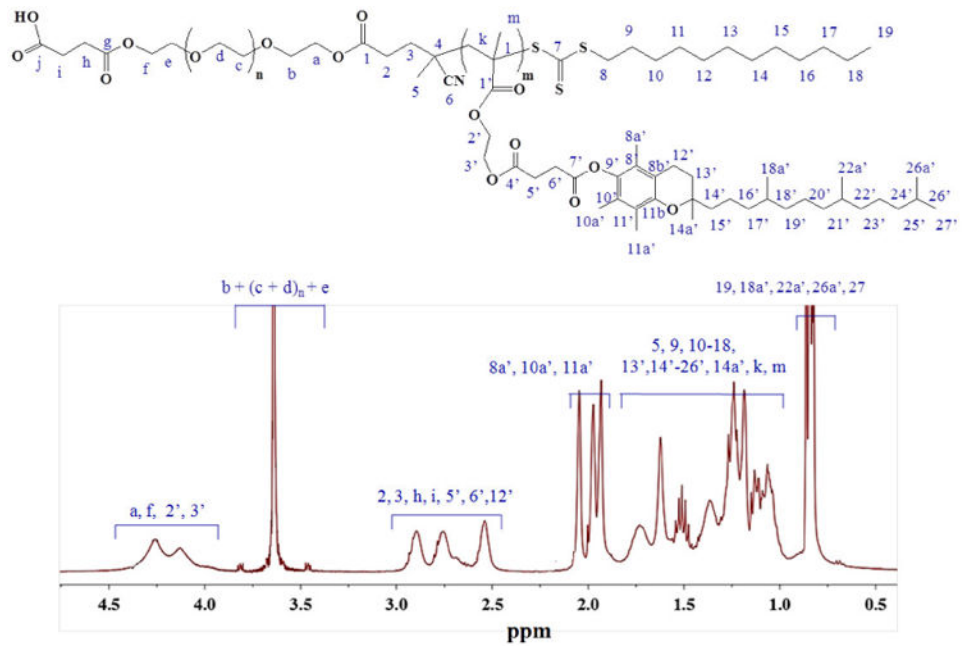


Figure 3.  $^1\text{H-NMR}$  spectrum of COOH-PEG-*b*-polyMTOS

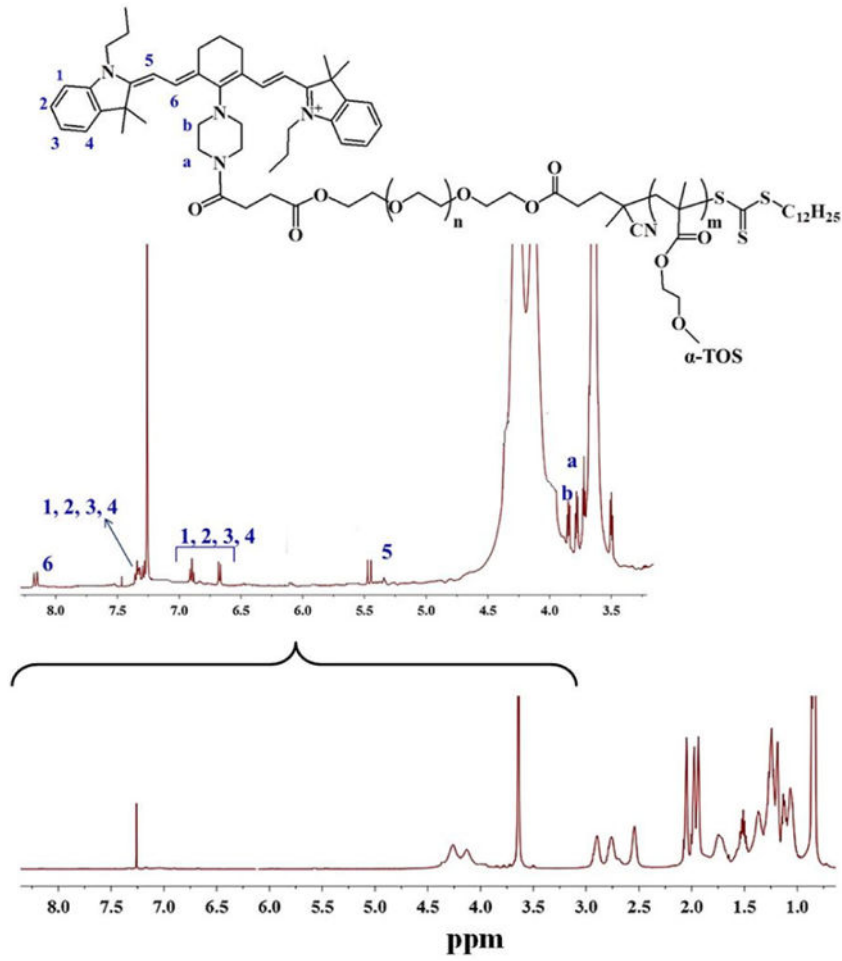
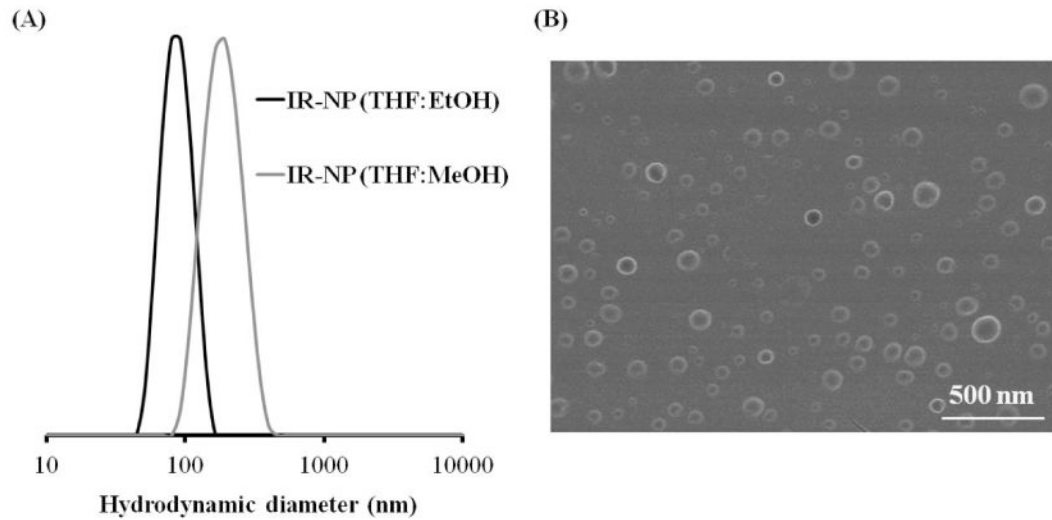
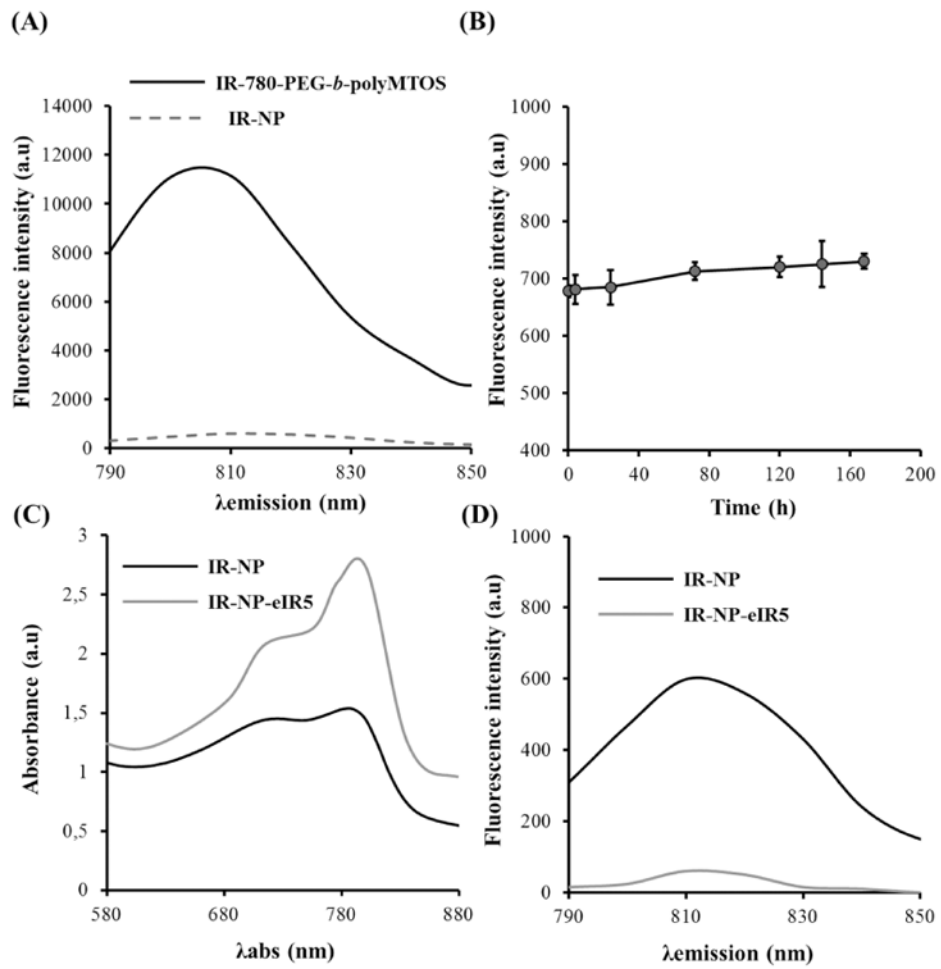


Figure 4.  $^1\text{H-NMR}$  spectrum of the polymeric conjugate IR-780-PEG-*b*-polyMTOS



**Figure 5.**

(A) Particle size distributions ( $D_h$  by intensity) of IR-NP as a function of the organic phase used during the SORP method using NaCl as aqueous phase in both cases, measured by Dynamic Light Scattering. Black: THF:EtOH; Grey: THF:MeOH. (B) SEM micrograph of IR-NP dried from aqueous suspension at RT. Scale bar: 500 nm.



**Figure 6.** (A) Fluorescence spectra of IR-780-PEG-*b*-polyMTOS conjugate and IR-NP after purification by dialysis. (B) Photostability of IR-NP at 37 °C. Comparison of absorbance (C) and fluorescence spectra (D) of IR-NP and IR-NP-eIR5.

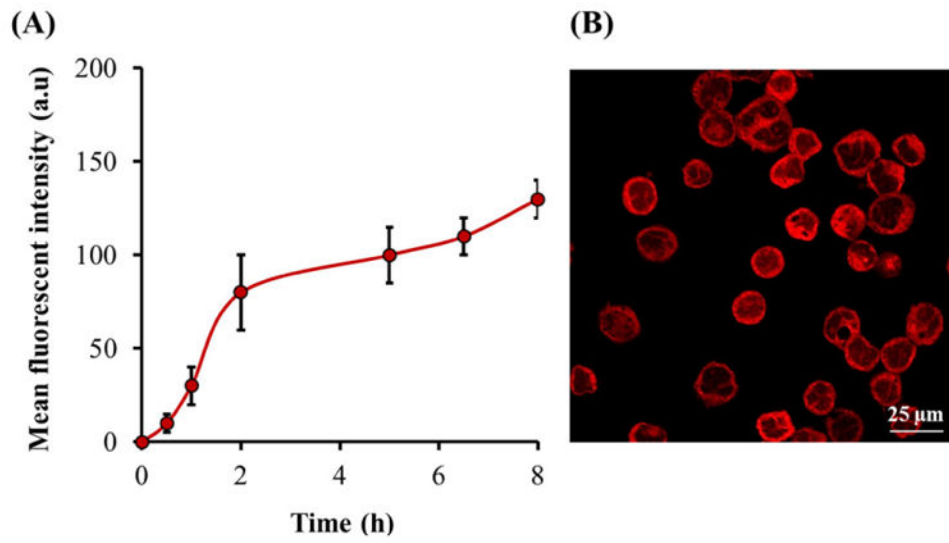


**Figure 7.** (A) Monitoring of cellular uptake of IR-NP (B) CLSM micrograph of MDA-MB-453 cells after 5 h of incubation with IR-NP at 1.5 mg/mL.

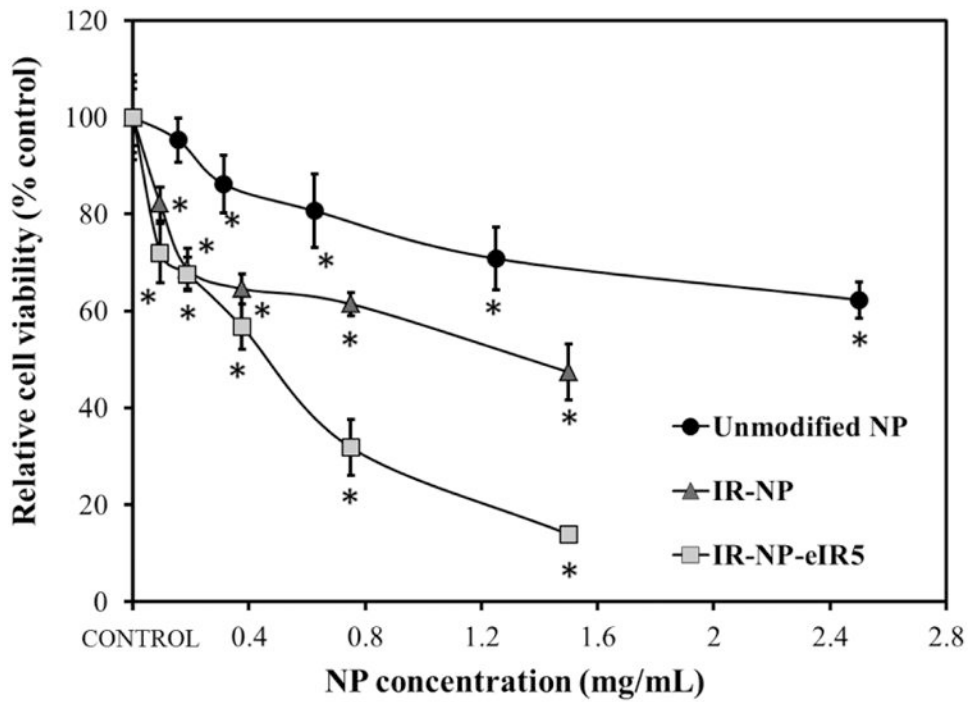


**Figure 8.** Viability of MDA-MB-453 cells incubated with indicated concentrations of unmodified-NP, IR-NP and IR-NP-5 for 24 h. Data are expressed as mean  $\pm$  S.D (n=8), and are relative to the metabolic activity of untreated cells (control). \*p<0.05 compared to control.



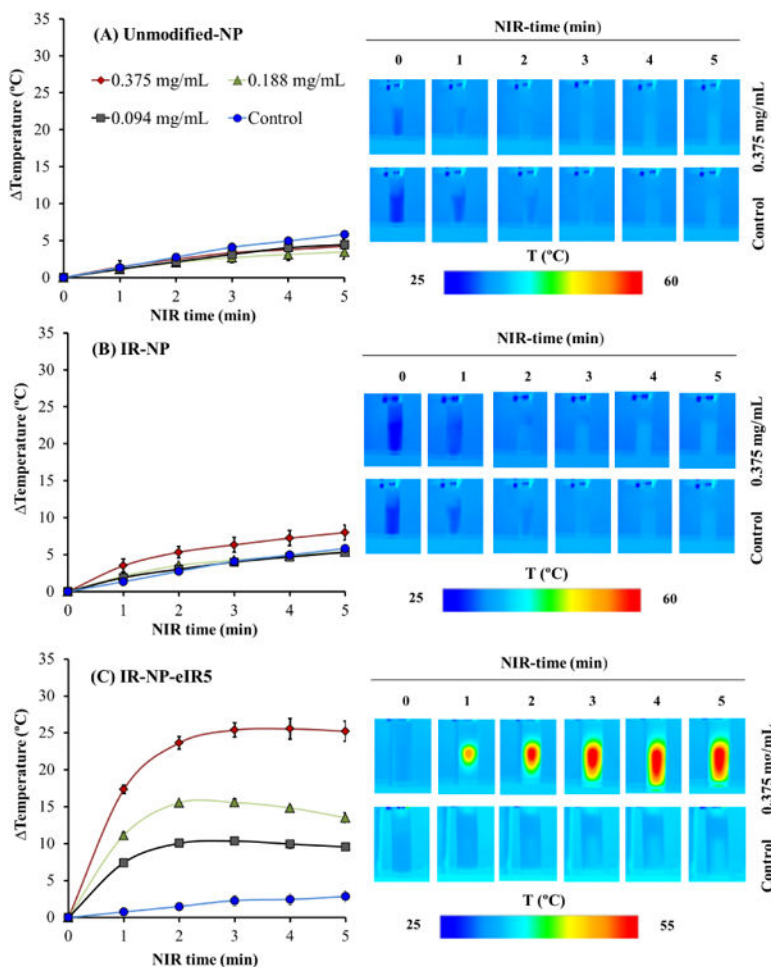


**Figure 9.** Photothermal properties of NPs based in the IR-780-PEG-*b*-polyMTOS conjugate. Aqueous suspensions containing the indicated dose of unmodified-NPs (A), IR-NP (B) or IR-NP-eIR5 (C) were exposed to NIR-laser for 5 minutes and monitored by IR-thermography at the indicated time points. The graph shows the maximum temperature rise detected in the sample during laser treatment. Images show the IR thermography of suspensions containing 0.375 mg/mL NPs or not (control) during NIR-treatment for the indicated times. Data are expressed as mean ± S.D (n=3).

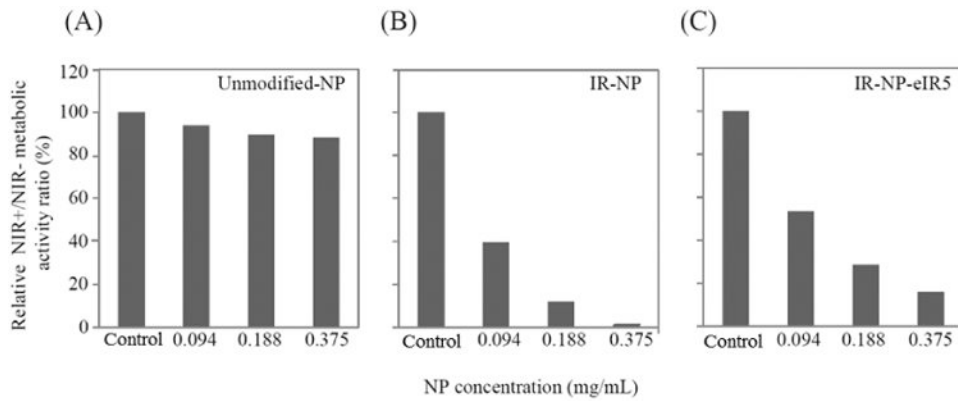


**Figure 10.** Metabolic activity of MDA-MB-453 cells incubated for 24 h with unmodified-NP (A), IR-NP (B) or IR-NP-eIR5 (C), then irradiated (+) or not (-) with NIR laser (NIR) for 10 min, washed twice with PBS, and further incubated at 37°C-5% CO<sub>2</sub> in fresh culture medium lacking NPs for 18 h. The data are expressed as the ratio between the metabolic activities of NIR+ and NIR- cultures, treated with the indicated dose of NPs, and are relative to the corresponding ratios of cell cultures not exposed to NPs (control) which were given a value of 100. One representative experiment of 3 independent experiments is shown.

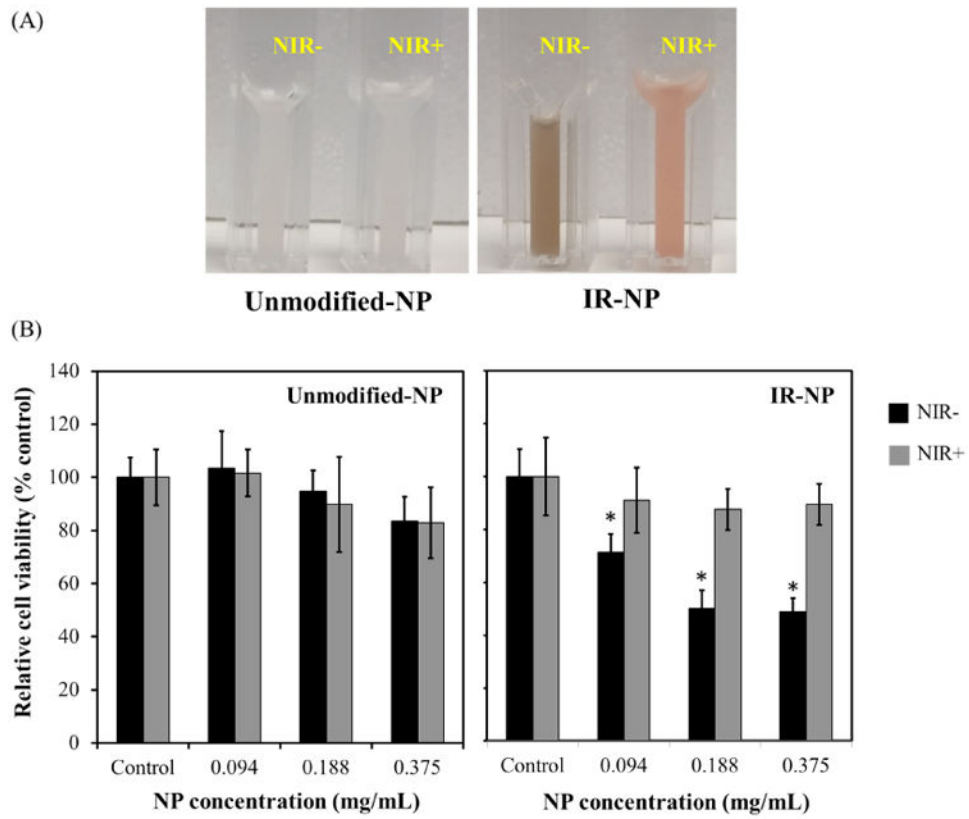


**Figure 11.**

(A) Photographs show NPs dispersions in 100 mM NaCl after irradiation (+) or not (-) with NIR-laser (NIR) for 10 min. (B) Graphs show the metabolic activity of MDA-MB-45 cells after incubation for 18 h with the indicated doses of NPs suspensions treated as in (A). Data are expressed as mean  $\pm$  S.D (n=3) and are relative to the metabolic activity of cultures not exposed to NPs (control). \*p<0.05 compared to control.

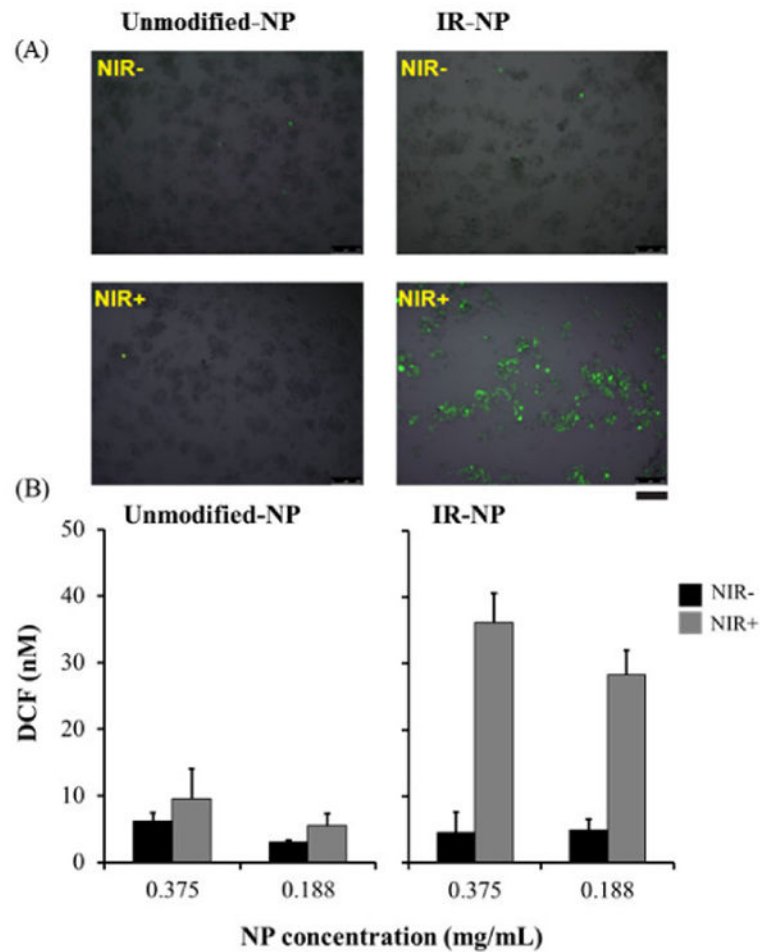


**Figure 12.**

(A) Epifluorescence micrographs of MDA-MB-453 cells, incubated for 24 h with 0.375 mg/mL unmodified-NP or IR-NP, loaded with DCFH and then illuminated (+) or not (control) with NIR-laser for 10 min (NIR). (B) Graphs show DCF levels in cell cultures incubated for 24 h with the indicated dose of unmodified-NP or IR-NP, loaded with DCFH and illuminated as in (A). Scale bar= 250  $\mu$ m.

Summary of most relevant structural characteristics of CTA-PEG<sub>8</sub>-COOH and COOH-PEG-*b*-polyMTOS block copolymer.

**Table 1**

Sample	a) $M_n \times 10^{-3}$	b) $M_{nSEC} \times 10^{-3}$	b) $\overline{D}$	a) $\eta_{PEG}$	a) $m_{MTOS}$	$f_{PEG-f_{MTOS}}$ (mol %)
CTA-PEG <sub>8</sub> -COOH	8.2	9.9	1.12	177	---	---
COOH-PEG- <i>b</i> -PolyMTOS	68.3	66.6	1.40	177	75	70-30

a) Determinated using <sup>1</sup>H-NMR spectroscopy

b) Determinated by SEC (THF) using PMMA standards

**Table 2**

Most relevant characteristics of unmodified-NP, IR-NP and IR-NP-eIR, including encapsulation efficiency (EE), hydrodynamic diameter ( $D_h$ , by intensity), polydispersity index (PDI); and zeta potential values ( $\zeta$ ).

NP sample	Organic phase	% Load	EE (%)	$D_h$ (nm)	PDI	$\zeta$ (mV)
Unmodified-NP	Dioxane	---	---	134.9 ± 6.5	0.079 ± 0.012	-2.4
IR-NP	THF:MeOH (50:50 v:v)	---	---	178.4 ± 11.8	0.187 ± 0.020	+3.1
IR-NP	THF:EtOH (50:50 v:v)	---	---	88.8 ± 6.7	0.058 ± 0.022	+2.9
IR-NP-eIR3	THF:EtOH (50:50 v:v)	3	85	110.2 ± 6.4	0.160 ± 0.017	+9.2
IR-NP-eIR5		5	89	134.6 ± 5.8	0.150 ± 0.012	+12.6
IR-NP-eIR10		10	92	167.2 ± 8.3	0.253 ± 0.023	+15.7